Biomaterials 35 (2014) 5056–5064

Contents lists available at ScienceDirect

Biomaterials

journal homepage: www.elsevier.com/locate/biomaterials

Force-driven evolution of mesoscale structure in engineered 3D microtissues and the modulation of tissue stiffening

Ruogang Zhao [a,*], Christopher S. Chen [b,1], Daniel H. Reich [a]

[a] Department of Physics and Astronomy, The Johns Hopkins University, 3400 North Charles Street, Baltimore, MD 21218, USA
[b] Department of Bioengineering, University of Pennsylvania, 510 Skirkanich Hall, 210 South 33rd Street, Philadelphia, PA 19104, USA

ARTICLE INFO

Article history:
Received 14 December 2013
Accepted 12 February 2014
Available online 12 March 2014

Keywords:
Soft tissue biomechanics
Engineered microtissue
Tissue structure
Magnetic actuation

ABSTRACT

The complex structures of tissues determine their mechanical strength. In engineered tissues formed through self-assembly in a mold, artificially imposed boundary constraints have been found to induce anisotropic clustering of the cells and the extracellular matrix in local regions. To understand how such tissue remodeling at the intermediate length-scale (mesoscale) affects tissue stiffening, we used a novel microtissue mechanical testing system to manipulate the remodeling of the tissue structures and to measure the subsequent changes in tissue stiffness. Microtissues were formed through cell driven self-assembly of collagen matrix in arrays of micro-patterned wells, each containing two flexible micropillars that measured the microtissues' contractile forces and elastic moduli via magnetic actuation. We manipulated tissue remodeling by inducing myofibroblast differentiation with TGF-β1, by varying the micropillar spring constants or by blocking cell contractility with blebbistatin and collagen cross-linking with BAPN. We showed that increased anisotropic compaction of the collagen matrix, caused by increased micropillar spring constant or elevated cell contraction force, contributed to tissue stiffening. Conversely, collagen matrix and tissue stiffness were not affected by inhibition of cell-generated contraction forces. Together, these measurements showed that mesoscale tissue remodeling is an important middle step linking tissue compaction forces and tissue stiffening.

1. Introduction

Organs and tissues exhibit complex and hierarchical structures. These structures determine the mechanical strength of the tissue and provide the foundation for tissues to perform their physiological functions [1,2]. In the effort to engineer artificial tissues for repairing damaged native tissues, one common approach is to cast cells and extracellular matrix (ECM) proteins in molds of specific geometries and then allow the tissue to form through a self-assembly process driven by the interplay between cell-generated forces and the mechanical boundary conditions [3–5]. This approach has proven effective in creating a range of engineered tissues that can mimic the macroscopic morphology as well as the ECM fibril-level microstructure of native tissues [6,7]. However, at intermediate mesoscopic scales in such tissues, it has been found that anisotropic clustering of cells and compaction of the ECM develops in local regions due to the mechanical constraints induced by the molds [7–10]. Since these mesoscale structures are intermediate building blocks for tissues' hierarchical architectures, they likely contribute to the strength of the tissues. However, how the formation of these structures is regulated and how changes in structure formation affect tissue strength is largely unknown.

Cells sense and react to mechanical cues from their surroundings. In engineered tissues, cell migration and ECM rearrangement are strongly influenced by the anisotropic mechanical boundary conditions imposed by the molds [6,11–13]. For example, cell populated collagen matrix that was adhered to a rigid substrate compacted through its thickness towards the anchorage substrate [14]. In cell populated collagen matrix anchored between two posts, the compaction of the matrix perpendicular to the anchoring axis led to the formation of two condensed collagen bands that were parallel with the axis [10,15,16]. Cell migration and clustering close to the outer surface of tubular tissue samples grown around a mandrel has also been reported [7,17]. However, while the anisotropic distribution of cells and ECM is a common effect, a quantitative understanding of the mechanical regulation of mesoscale

* Corresponding author. 332 Bonner Hall, Department of Biomedical Engineering, University at Buffalo, The State University of New York, Buffalo, NY 14260, USA. Tel.: +1 716 645 1034.
E-mail address: rgzhao@buffalo.edu (R. Zhao).
[1] Current address: Department of Biomedical Engineering, Boston University, Boston, MA 02215, USA.

http://dx.doi.org/10.1016/j.biomaterials.2014.02.020
0142-9612/

structure formation is still lacking due to the difficulties in monitoring cell generated forces during tissue remodeling and in varying the mechanical boundary conditions in 3D. Furthermore, even though the tissue stiffness was measured in some previous studies [5,7,15], the evaluation of the structure–strength relationship has focused on microscale properties. As a result, it is unclear what role the mesoscale structure plays in modulating the stiffening of these tissues.

Another technical challenge that hinders the study of mesoscale structures is the size of conventional engineered tissues, which are typically on centimeter scales [16,18]. At this length scale, only a small region of the tissue sample can be visualized through high magnification microscopy. As a result, a full map of the mesoscale structure has not been obtained. The recent emergence of microfabricated 3D biomaterials systems may provide a potential solution for this problem. Bioprinting techniques [19,20] and photolithography-based patterning techniques [13,21] have been used to build 3D tissues that are of millimeter and even smaller length scales. The small size of these microtissues enables the study of structural remodeling from micro to macroscopic tissue levels. More recently, we have developed a magnetic microtissue tester (MMT) system that enables mechanical actuation of microtissues formed between pairs of poly(-dimethylsiloxane) (PDMS) micropillars, allowing *in situ* measurement of both tissue contraction force and tissue stiffness during tissue remodeling [22]. Furthermore, the feasibility of using such a system to detect microtissue structure has also been validated [23,24]. With its combined capabilities of mechanical testing and mapping of tissues' micro to macroscale structures, this system has the potential to be used for the study of the structure–mechanics relationships of engineered tissues.

The objective of this study was to understand how the remodeling of mesoscale structure is regulated and subsequently how this remodeling affects tissue stiffening. To answer this question, we utilized the magnetic microtissue tester system to vary several factors that have been previously shown to affect tissue remodeling, including the phenotype of the embedded cells [25], the mechanical boundary conditions [26], the tissue contractility and the cross-linking of the ECM in the tissue [27,28]. We examined how these factors affected the remodeling of the microtissues' structure, their impact on the microtissues' stiffness, and the correlation between tissue remodeling and tissue stiffening.

2. Materials and methods

2.1. Magnetic microtissue tester system

The fabrication of arrays (10 × 13) of PDMS (Sylgard 184, Dow-Corning) microwells containing pairs of micropillars was performed as previously described (Fig. 1A) [22,29]. To study of the effects of micropillar spring constant on microtissues' properties, the spring constant of the micropillars was varied by changing the elastic modulus of the PDMS. Soft, intermediate and stiff micropillars were made from PDMS with elastic modulus of 0.54 MPa, 1.6 MPa and 4.0 MPa, respectively, by varying the PDMS/curing agent ratio. This yielded micropillars with effective spring constants for small deflections of $k = 0.3$, 0.9, and 2.2 μN/μm, respectively. The mesoscale structure and the mechanical properties of microtissues grown with these different micropillar boundary conditions were compared after 3 days of culture. Except as otherwise noted, the experiments were carried out using the intermediate stiffness micropillars.

To enable magnetic actuation of the microtissues, a nickel sphere with ~100 μm diameter (CAS 7440-02-0, −150 + 200 mesh, Alfa Aesar) was adhered to one pillar in each microwell [22]. Actuation of individual magnetic pillars was achieved by applying a ramped magnetic field using a custom-made micromanipulator-controlled electromagnetic tweezer with a sharpened pole tip, which could be brought in close proximity to the Ni sphere (Fig. 1B). During magnetic pillar actuation, changes in the magnetic field and image acquisition were synchronized under computer control.

2.2. Microtissue seeding and culture

Microtissues were seeded by introducing a suspension of NIH 3T3 fibroblasts and 2.5 mg/mL unpolymerized rat tail collagen type I (BD Biosciences) into the PDMS microwells as previously described [22]. Immediately after seeding, the microtissue tester device was kept at 37 °C for 9 min to allow collagen polymerization. Microtissue culture was maintained up to 3 days in high glucose DMEM containing 10% bovine serum, 100 units/mL penicillin, and 100 mg/mL streptomycin (all from Invitrogen). Cell proliferation was examined by counting cell numbers in the microtissue. We detected cell proliferation from day 1 to day 3 (Supplemental Fig. S5).

2.3. Microtissue contraction force and stiffness measurements

The spontaneous contraction force generated by individual microtissues and their stiffnesses were measured as previously described [22]. Briefly, a microtissue's contraction force F' was determined from the average deflection of the two micropillars, as measured by phase contrast microscopy, comparing the deflected position of the centroid of each pillar top with the centroid of its base. The contraction stress was calculated as $\sigma' = F'/A$, where A is the cross-sectional area of the center of the microtissue. Where the micropillars' bending exceeded the small deflection regime, such as in the soft pillar and TGF-β1 treated conditions, a finite element analysis-derived nonlinear load–deformation relationship for the micropillars was used to calculate the tissue force (Supplemental material).

Each microtissue's stiffness was measured through a magnetically actuated stretching test as previously described [22]. During stretching of the microtissue, the increasing tensile force $F = k\delta$ on the microtissue was determined from the deflection δ of the non-magnetic pillar. The engineering stress of the microtissue was calculated as $\sigma = F/A$. The strain over the central region of the microtissue was determined based on sequential phase contrast images obtained during stretching, using a texture correlation image analysis algorithm [30]. The tensile elastic modulus of the central region was taken as the slope of the engineering stress–engineering strain curve. The contraction force and stiffness of microtissues were measured after each pharmacological treatment performed in the current study.

2.4. Pharmacological treatments

To induce fibroblast differentiation to myofibroblasts in the microtissues, regular culture media was supplemented with 5 ng/mL of TGF-β1 (T7039, Sigma) continuously for 3 days. TGF-β1 is a potent stimulator for myofibroblast differentiation [28,31]. To inhibit collagen cross-linking during microtissue formation and culture, 3-aminopropionitrile fumarate salt (BAPN, A3134, Sigma) was added to the microtissue cultures at 50 μg/mL, 100 μg/mL or 1 mg/mL concentrations immediately after seeding, and maintained for 3 days. BAPN is an inhibitor of lysyl oxidase, an enzyme required for collagen cross-linking [32–34]. Microtissues were treated with 2 μM, 5 μM or 10 μM of blebbistatin (B0560, Sigma) in a similar manner to inhibit cell contractility during microtissue formation and the subsequent 3 days of culture. To separate cell and ECM contributions to the mechanical properties of TGF-β1 treated microtissues, microtissues were treated with 0.5% Triton X-100 for 15 min which we have previously shown is sufficient to kill all the cells in such microtissues [22].

2.5. Immunofluorescence, microscopy, and image analysis

Myofibroblast specific biomarkers, α-smooth muscle actin (α-SMA) and ED-A fibronectin (EDA-Fn), were labeled using immunofluorescence techniques and detected using confocal microscopy. To preserve the delicate α-SMA fibers in these 3D microtissues, a modified detergent-free staining protocol was used [35]. Microtissues were fixed with 1% paraformaldehyde in PBS, permeabilized with cold methanol at − 20 °C for 3 min, incubated with primary antibodies against α-SMA (clone 1A4, A2547, Sigma), rat collagen type-1 (AB755P, Millipore) or mouse ED-A fibronectin (IST-9, ab6328, Abcam), labeled with fluorophore-conjugated, anti-IgG antibodies (AlexaFluor, Invitrogen) and counterstained with Hoechst 33342 (Invitrogen). Due to the antibodies' species specificity, the antibody for rat collagen type-1 (AB755P, Millipore) only labeled collagen that was introduced during the seeding process and the antibody for mouse ED-A fibronectin (IST-9, ab6328, Abcam) only labeled fibronectin that was produced by seeded mouse 3T3 cells [23]. This allowed us to detect the spatial distribution of originally seeded ECM component and cell produced ECM component.

The microtissues were imaged on a Zeiss LSM-510 Meta confocal microscope with a Plan-Apochromat 20× air objective in 1.5 μm optical slices for all channels. For each microtissue imaged, a 450 μm × 209 μm area was scanned through an approximately 80 μm thickness with 4× line averaging. The stack of images was then processed using the 3D Viewer tool in ImageJ (NIH) to obtain the 3D reconstructed views. To track the micropillar bending and microtissue deformation during tensile testing, individual microtissues were imaged on a Nikon TE2000-E motorized microscope with a Plan-Fluor 10× objective using a CoolSNAP-HQ camera (Photometrics, Tucson, AZ). Samples were maintained at 37 °C during live cell imaging.

3. Results

3.1. Tissue stiffening during early microtissue formation

Immediately after microtissue seeding, the process of collagen polymerization caused the formation of solid homogeneous

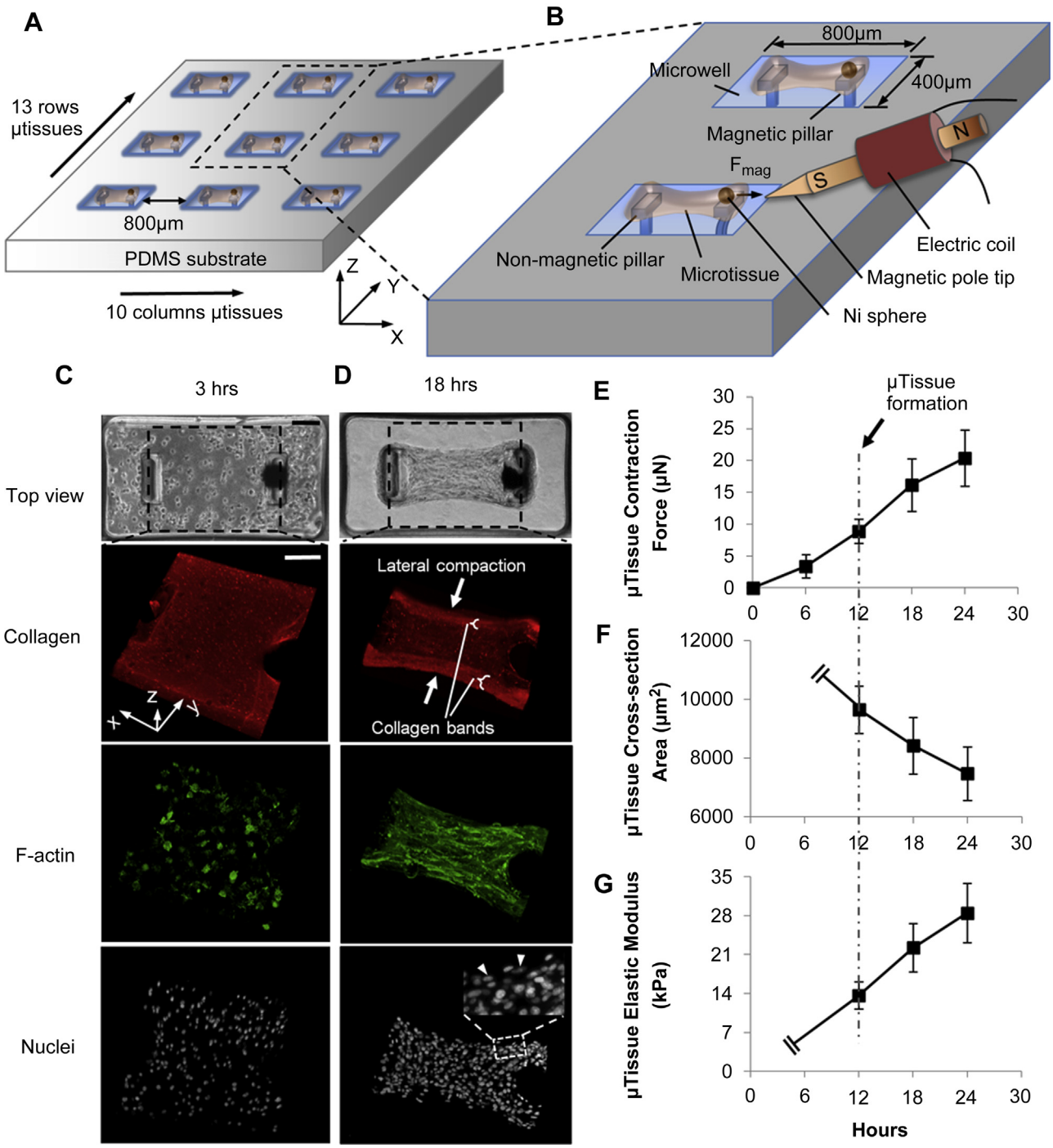

Fig. 1. Schematic of the magnetic microtissue testing (MMT) system and the mechanical parameters associated with the early stage anisotropic compaction of the microtissues (µtissue). (A) Arrays of fibroblast populated 3D microtissues were formed through self-assembly in microwells containing paired microcantilevers. (B) The microtissues' elastic modulus was measured through magnetically actuated tensile testing on individual microtissues. (C) A homogeneous collagen gel with uniformly distributed cells formed in a microwell after seeding. Collagen, F-actin and Nuclei images are 3D views reconstructed from confocal stacks. (D) Cellular forces drove lateral compaction of the collagen matrix into bands on unconstrained edges by 18 h. Confocal images in (C) and (D) cover the dashed rectangles in the corresponding phase images. Arrowheads indicate cell nuclei elongated along the contraction direction. The increase of the microtissues' contraction force (E) and the decrease of the cross-sectional area (F) were accompanied by an increase of the elastic modulus (G) within 24 h. Scale bar = 100 µm. Sample size for each condition: $n = 9$, All data are presented as Mean ± S.D.

collagen gels with uniformly embedded cells in each microwell (Fig. 1C). As shown in Fig. 1D, several hours after seeding, the encapsulated cells caused the collagen gel in each well to compact and form a dog-bone shaped microtissue suspended between the two micropillar heads. During this process, the cell-generated contraction forces were balanced by the micropillars in the longitudinal direction (x-direction) of the microtissues, but were able to freely compact the collagen matrix in the lateral direction. As a result, we observed the consolidation of the collagen matrix after 18 h in culture into band-like structures on the unconstrained edges of the microtissues, with less compacted regions in the centers. We found that F-actin stress fiber bundles and elongated

cell nuclei in the collagen band regions aligned predominantly along the longitudinal axis of the tissue, indicating the existence of an anisotropic tension field as a result of the interaction between cell-generated contraction forces and the constraint of the micropillars (Fig. 1D). We measured the microtissues' elastic modulus through magnetically actuated tensile testing of the individual microtissues (Fig. 1B). The microtissues' elastic modulus, cross-sectional area and contraction force were monitored within a 24-h period. We observed the formation of many dog-bone shaped microtissues 12 h after seeding, and continuous increase of the contraction force through 24 h (Fig. 1E), as seen previously [29]. From 12 h to 24 h, the cross-sectional area of the microtissues kept decreasing (Fig. 1F), and the collagen bands converged laterally towards the tissue center. This trend was accompanied by an increase in the microtissues' elastic modulus over the same period (Fig. 1G).

3.2. Microtissue stiffening modulated by myofibroblast differentiation

Over longer culture periods, we manipulated the evolution of the microtissues' structure by inducing fibroblast differentiation to myofibroblasts (a phenotype that is more contractile and produces more ECM [28,31]) via treatment with TGF-β1. As shown in Fig. 2A, in both the serum-only and TGF-β1 treated conditions, we observed the formation of sparse α-SMA stress fiber bundles at day 1, and increased fiber bundle density and the formation of an interwoven α-SMA fiber meshwork by day 3. However, compared to the serum-only condition, the α-SMA stress fiber bundles in the TGF-β1 treated case were much thicker and denser at both day 1 and day 3, respectively, indicating elevated levels of myofibroblast differentiation in these microtissues (Fig. 2A, α-SMA; Supplemental Figs. S2, S4A,B and S6; Movies S1–S2). A similar pattern was also observed in the expression of cell produced ED-A fibronectin (ED-A Fn) for day 3 tissues (Supplemental Fig. S3; Movies S5–S6). The cross-section of the day 3 microtissues was found to be oval with cells covering the microtissues' top surface to form an outer shell that predominantly expressed α-SMA and ED-A Fn (Supplemental Figs. S2 and S3, Cross-section view). This was found to be consistent with previous observations [23]. As expected, the TGF-β1 treated microtissues caused much larger bending of the micropillars (Fig. 2A, side view) than serum-only treated microtissues at both day 1 and day 3, indicating that they were generating much larger forces. Due to the shortened distance between the two micropillar heads and the relatively constant collagen volume in each microwell, the cross-sectional area of the TGF-β1 treated microtissues was much larger than those cultured only in serum (Fig. 2C; Supplemental Fig. S4C,D) and the cell density was higher at day 3 (Supplemental Fig. S4E,F). The contraction stress of the TGF-β1 treated microtissues was more than 150% higher than that of the serum-only treated microtissues at day 1 and day 3, respectively (Fig. 2D).

Supplementary video related to this article can be found at http://dx.doi.org/10.1016/j.biomaterials.2014.02.020.

As shown by the collagen images in Fig. 2A, we observed lateral convergence of the collagen bands and increased band width, as well as decreased cross-sectional area of the microtissues (Fig. 2C) between day 1 and day 3 in the serum-only condition, indicating continued lateral compaction. This trend correlated with an increase in microtissue stiffness by 20% during the same period (Fig. 2E). The collagen structure of the TGF-β1 treated microtissues at day 1 was similar to that of the serum-only condition but was shorter longitudinally, due to the strong contraction in this direction. By day 3, the collagen bands in the TGF-β1 treated samples converged significantly and merged with the collagen matrix in the tissue center to form a dense core structure (Fig. 2A, Collagen). On top of this core, as noted above, differentiated myofibroblasts co-localized with a layer of type I collagen and abundant ED-A Fn (Supplemental Fig. S3; Movies S5–S6). This outer shell of cells and ECM integrated with the collagen core to form a composite structure (Supplemental Fig. S3, Cross-section view). We found that this elevated compaction and reinforcement of the collagen structure by the myofibroblasts correlated with a significant increase in the tissue stiffness. The elastic modulus of the TGF-β1 treated microtissues was 20% and 64% higher than that of the serum-only treated microtissues at day 1 and day 3, respectively.

To further elucidate the role of mesoscale collagen structure in modulating tissue stiffness, we performed acute Triton-X treatment for 15 min on TGF-β1 treated day 3 microtissues. The Triton-X treatment caused significant reduction in the contraction force and stress (Fig. 2B, D) but almost no change in the microtissues' elastic modulus (Fig. 2E), indicating that the tissue stiffness was determined by the collagen structure, consistent with our previous observations in serum-only conditions [22]. Notably, relatively high contraction forces remained after the Triton-X treatment, indicating that a high degree of collagen compaction was preserved, likely due to the development of significant level of cross-linking in these composite collagen structures by day 3.

3.3. Modulation of microtissue stiffening by micropillar boundary conditions

We also manipulated the structural evolution of the microtissues by varying the mechanical constraints applied to them. As shown by the side view images in Fig. 3A, we found that the deflection of the micropillars caused by the microtissue contraction was inversely proportional to the pillar spring constant, indicating that the microtissues generated essentially the same contraction forces for each of the three boundary conditions (Fig. 3B). However, the microtissues' cross-sectional area decreased significantly on the stiffer pillars (Fig. 3C), leading to increased contraction stress (Fig. 3D). As shown by the collagen images in Fig. 3A, the mesoscale collagen structures of microtissues cultured under the three different mechanical boundary conditions were distinct. We found increased lateral convergence of the collagen bands with increased micropillar spring constant. Compared to the stiff pillar case, the collagen matrix between the bands in the soft pillar case appeared to be less compacted. This mechanical constraint-guided lateral compaction of the collagen structure was found to correlate with the elastic modulus of the microtissues, which increased strongly with increasing micropillar spring constant (Fig. 3E). We did not observe significant differences in the expression of myofibroblast markers between microtissues grown under different mechanical constraints (Supplemental Figs. S2 and S3; Movies S3–S4, S7).

Supplementary video related to this article can be found at http://dx.doi.org/10.1016/j.biomaterials.2014.02.020.

3.4. The effects of inhibition of collagen cross-linking and cellular contractility on microtissue stiffening

Since cellular contraction is one of the main drivers for structural evolution of the microtissues, and collagen cross-linking has been reported to affect tissue stiffness [27], we inhibited these two processes with blebbistatin and BAPN treatments, respectively, during microtissue formation and over three days of culture to study their effects on collagen structural evolution and tissue stiffening. As shown in Fig. 4A, neither treatment caused obvious cross-sectional area change of the microtissues as compared to untreated controls, except for 10 μM blebbistatin where dog-bone shaped microtissues did not form, likely due to strong inhibition of cell contractility at this

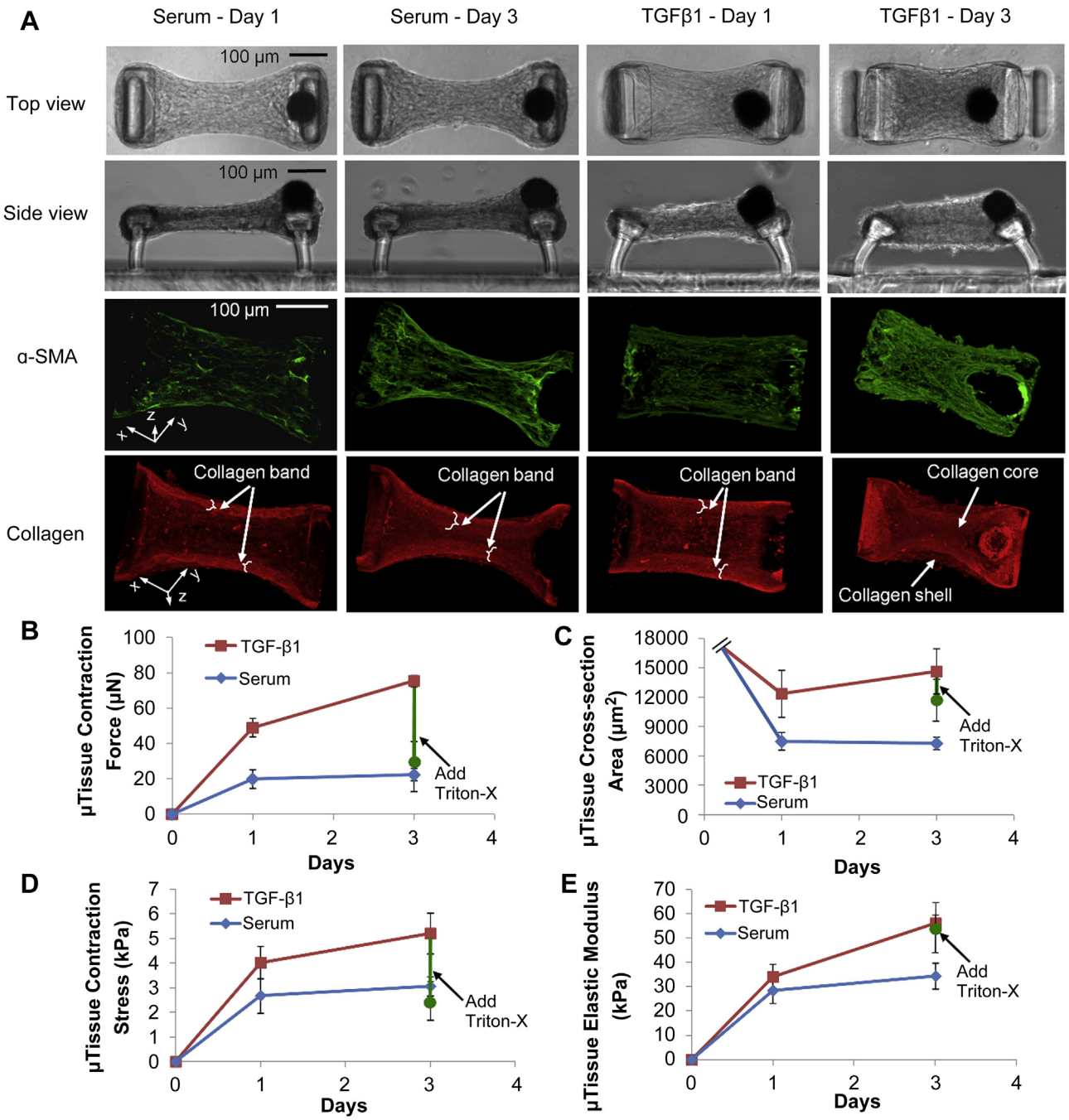

Fig. 2. Increased lateral convergence of the collagen bands and reinforcement of the collagen structure caused by differentiated myofibroblasts correlated with significant microtissue stiffening. TGF-β1 treatment caused significant increase in cross-sectional area (A, Top view and Side view; C), micropillar deflection (A, Side view), α-SMA stress fiber thickness and density (A, α-SMA), contraction force (B), and contraction stress (D) of the microtissues at both day 1 and day 3 as compared to serum-only treatment. From day 1 to day 3, the lateral convergence of the collagen bands in the serum-only condition (A, Serum—Collagen) correlated with the increase in elastic modulus (E, Serum). The formation of a dense collagen core structure due to increased lateral convergence of the collagen bands and the reinforcement of this structure by differentiated myofibroblasts (A, TGFβ1—Collagen) correlated with significant tissue stiffening as compared to serum-only condition (E, TGF-β1). Triton-X treatment caused significant reduction in the contraction force and stress but almost no change in the elastic modulus (B—E). Collagen and α-SMA images are 3D views reconstructed from confocal stacks. Sample size for each condition: $n > 9$. All data are presented as Mean ± S.D.

concentration [35]. At lower blebbistatin concentrations (2 μM and 5 μM), we observed a dosage dependent inhibition of the microtissues' contraction force (Fig. 4B), but no significant alteration in the collagen structure (Fig. 4A) and stiffness (Fig. 4C) as compared to untreated samples. α-SMA staining of the microtissues (Fig. 4A) and monolayers of cells seeded on coverslips (Supplemental Fig. S7) showed that low blebbistatin concentration did not significantly reduce the α-SMA expression [35], indicating there were still sufficient numbers of contractile cells to drive collagen structural remodeling. The lower dosage BAPN concentrations (50 μg/mL and 100 μg/mL) did not cause significant change in the microtissues' collagen structure (Fig. 4A), contraction force (Fig. 4B) or stiffness (Fig. 4C). However, at 1 mg/mL BAPN, we found that the microtissue surface was ruffled and the collagen structure was less continuous (Fig. 4A). Microtissues with this partially impaired collagen structure showed a 25% reduction in stiffness (Fig. 4C).

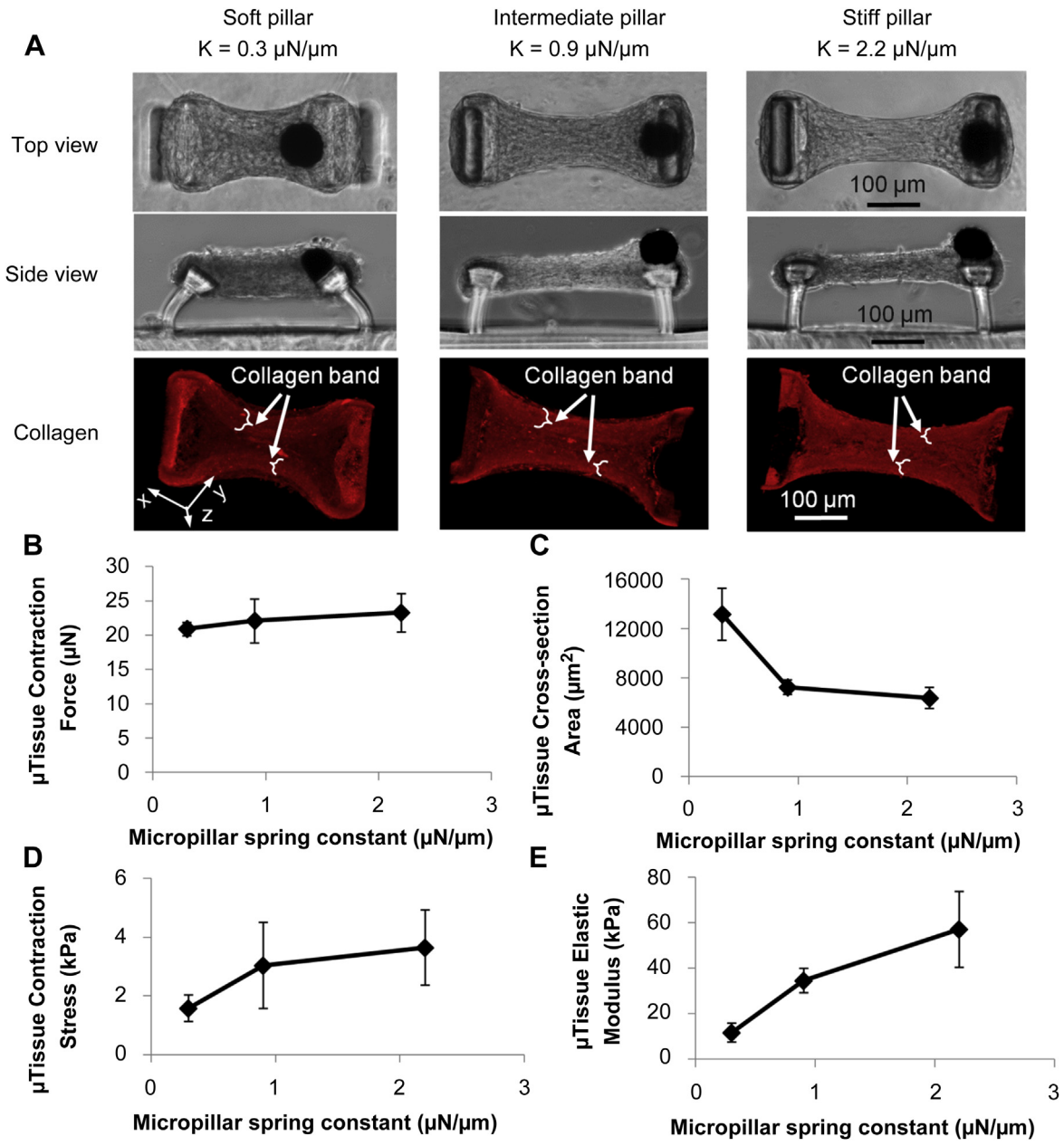

Fig. 3. Increased lateral convergence of the collagen bands on stiffer micropillars correlated with significant microtissue stiffening. The deflection of micropillars caused by the microtissue contraction is inversely proportional to the pillar spring constant (A, Top view, Side view), indicating that the microtissues generated essentially the same contraction forces for each of the three boundary conditions (B). Decreased microtissues' cross-sectional area on the stiff pillars (A, Top view, Side view; C) led to increased contraction stress (D). Lateral convergence of the collagen bands increased significantly from soft pillar to stiff pillar (A, Collagen), which corresponded to 190% and 410% increase in microtissue's elastic modulus for intermediate and stiff pillars, respectively (E). Collagen images are 3D views reconstructed from confocal stack. Sample size for each condition: $n > 9$. All data are presented as Mean ± S.D.

3.5. The role of mesoscale structure in tissue stiffening

To compare the contributions of cell-generated compaction force and mesoscale structural remodeling to microtissue stiffening, we plot the stiffness of the microtissues under BAPN treatment, blebbistatin treatment, no treatment, soft pillar and stiff pillar boundary conditions against cross-sectional stress (Fig. 5A) and cross-sectional area (Fig. 5B). Here the cross-sectional area is used as a quantitative measurement of the mesoscale structure. It can be seen that both inhibition of cell contraction force (blebbistatin) and the soft pillar boundary condition caused reduction in the cross-sectional stress (Fig. 5A). However, only the soft pillar condition caused both a significant change in the tissue mesoscale structure (cross-sectional area) and a corresponding reduction in stiffness (Fig. 5B). As a result, the correlation between the microtissue stiffness and the mesoscale structure is stronger (Fig. 5B, $R^2 = 0.68$) as compared to the correlation between the microtissue stiffness and the cell-generated compaction stress (Fig. 5A, $R^2 = 0.44$). Given that force driven structural remodeling precedes stiffening, these comparisons suggest that while cell-generated contraction forces are important, they alone are not enough to determine the tissue stiffness, and that mesoscale structural remodeling is an important middle step linking tissue compaction forces and tissue stiffening. The same argument also applies to the

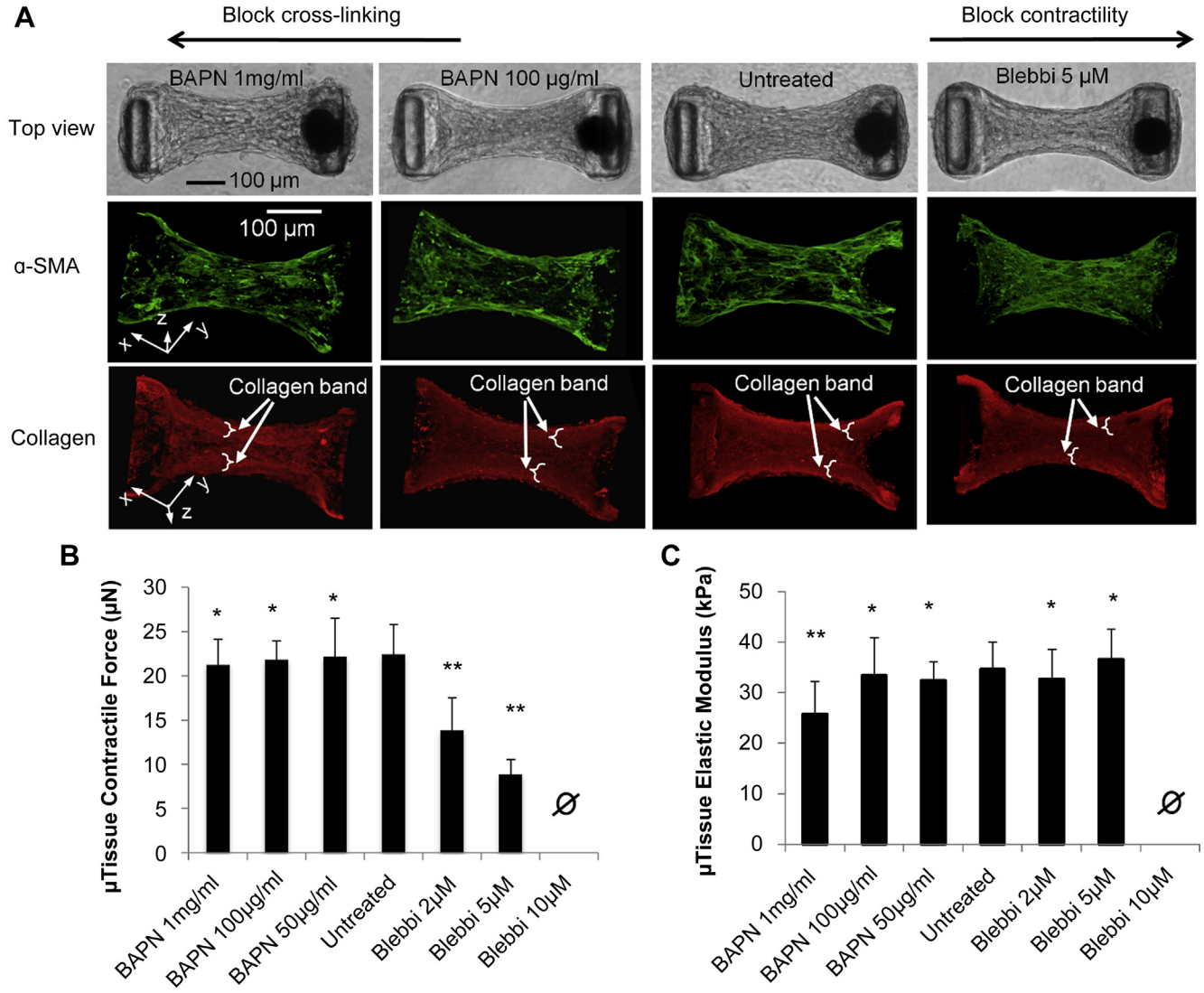

Fig. 4. Mesoscale structure formation and microtissue stiffness were not significantly altered by inhibiting collagen cross-linking or cellular contractility. Inhibition of microtissues' contraction force (B) using low dosage blebbistatin (Blebbi) (2 μM and 5 μM) or inhibition of collagen cross-linking using low dosage BAPN (50 μg/mL and 100 μg/mL) did not significantly affect the microtissues' cross-section area, α-SMA expression, collagen structure (A) or the elastic modulus (C). Under high BAPN concentration (1 mg/mL), the collagen structure is less continuous (A) and the microtissue elastic modulus reduced by 25% (C). The collagen and α-SMA images are 3D views reconstructed from confocal stacks. Sample size for each condition: $N > 9$. $^{**}p < 0.003$; $^{*}p > 0.16$ as compared to untreated condition by unpaired t-test. All data are presented as Mean ± S.D.

TGF-β1 treated conditions where significantly remodeled structure, including the formation of an ECM-rich outer shell, determined the tissues' stiffness.

4. Discussion

In this paper, we studied the mesoscale structure–mechanics relationship of 3D cell-populated collagen microtissues. Utilizing the MMT system, we pharmacologically and mechanically manipulated the formation of the mesoscale structure in microtissues, and simultaneously measured the cell-generated contraction forces, the tissues' mesoscale structure and the tissues' stiffness. We showed that anisotropic compaction of the collagen matrix, due to the constraints at the microtissues' ends provided by the micropillars, led to the formation of collagen bands on the unconstrained side edges of the microtissues. With increased micropillar spring constant or elevated cell contraction force, the collagen bands converged progressively along the tissues' perpendicular axis towards the tissue center. This evolution of mesoscale structure correlated with the increase of tissue stiffness. Conversely, when cell-generated contraction forces were inhibited, the mesoscale structure was not altered, and the stiffness remained the same. Together, these measurements provided quantitative examination of the driving forces and the tissue stiffening during mesoscale structural remodeling. Such systematic understanding of the mechanical events involved in tissue remodeling can help to improve not only the study of morphogenesis in native tissues but also the design and fabrication of engineered tissues.

Engineered tissue is a promising solution to restore the functionality of damaged organs. However, despite many years of intensive research in this field, most engineered tissues still only possess simple geometries that do not recapitulate the complicated geometry of many natural organs [3,5]. Studies of embryogenesis have shown that even though the development of complex body geometry is under strict genetic control, it is the mechanical force that brings all the parts into place [36]. Thus, understanding the

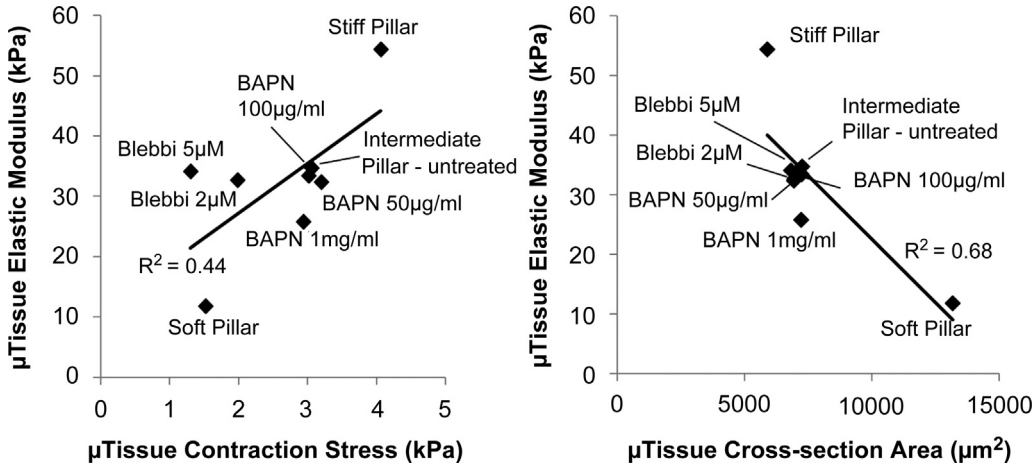

Fig. 5. Mesoscale structural remodeling is an important middle step linking tissue compaction forces and tissue stiffening. Elastic modulus is more weakly correlated with contraction stress (A, $R^2 = 0.44$) than with mesoscale structure (cross-sectional area) (B, $R^2 = 0.68$), indicating that cell-generated compaction forces alone are not enough to determine the tissue stiffness, and the mesoscale structural remodeling is an important middle step linking tissue compaction forces and tissue stiffening.

mechanism and further controlling the process of structural remodeling are important steps towards engineering functional tissues. In the current study, we demonstrated the mechanical causes for structural remodeling and its consequences for the mechanical properties of a widely used, dog-bone shaped tissue model [10,15,16,37]. Although this model is structurally specific, we expect that the underlying mechanism revealed is widely applicable to other engineered tissue systems. Specifically, since many engineered tissues are cultured under some type of mechanical constraint, the mechanical boundary condition and tissue stiffness relationships demonstrated here can be used as guidelines for controlling the evolution of hierarchical structure and stiffness in artificially grown tissues.

Cell mediated tissue compaction and cross-linking of ECM fibrils have been proposed as two principal mechanisms that cause tissue stiffening [27]. In the current study, our results suggest that anisotropic compaction of the collagen matrix may be an important cause of stiffening for early-age quiescent-cell (without added TGF-β1) populated engineered tissues (Fig. 2, serum-only; Figs. 3 and 4). Cross-linking of collagen fibrils may not be the main cause of stiffening for these tissues, as low concentration BAPN did not affect tissue stiffness and high concentration BAPN only induced 25% reduction in the tissue stiffness (Fig. 4), which is a much smaller impact as compared to that induced by varying the mechanical constraints (Fig. 3). A potential reason for this is that lysyl oxidase, an enzyme that catalyzes cross-linking of collagen, only slightly cross-links reconstituted collagen because such collagen is already well cross-linked before extraction from the animals [10]. Cross-linking is likely important, however, to the stiffness of TGF-β1 treated tissues (Fig. 2, TGF-β1). In these microtissues, differentiated myofibroblasts produced large amounts of ECM that are cross-linkable (Supplemental Fig. S3, EDA-Fn). Our Triton-X treatment results, which show that significant amount of ECM compaction remained after abolishing the cell contraction, support this hypothesis (Fig. 2, Add Triton-X). This hypothesis is also partially supported by previous observations that showed that engineered tissues subjected to prolonged culture period, which permitted the production of large amount of cross-linkable ECM, developed high stiffness [37].

In the current study, by continuously inhibiting cell contraction force or collagen cross-linking, we showed that cellular contractility is the primary driver of tissue tension, and that compacted collagen mesoscale structure predominantly determines the tissue stiffness. This finding is consistent with previous findings based on acute pharmacological treatments [22,38]. In TGF-β1 treated conditions, differentiated myofibroblasts became highly contractile and bio-synthetic and caused significant collagen compaction and stiffening. These events begin to simulate the mechanobiological processes of pathological wound healing [31], suggesting that, with its combined mechanical and biological capacities, the current microtissue testing system can be easily adapted for fibrotic disease and wound healing studies.

5. Conclusion

By dynamically manipulating the remodeling of microfabricated tissues using a novel magneto-mechanical testing system, we showed that increased anisotropic compaction of the intermediate length-scale (mesoscale) structures of the microtissue contributed to tissue stiffening, and that mesoscale remodeling is an important middle step linking tissue compaction forces and tissue stiffening. Such systematic understanding of the mechanical events involved in tissue remodeling can help to improve not only the study of morphogenesis in native tissues but also the design and fabrication of engineered tissues.

Acknowledgments

This work was supported in part by National Institute of Health grant HL90747. Confocal microscopy was performed at the JHU Integrated Imaging Center.

Appendix A. Supplementary data

Supplementary data related to this article can be found at http://dx.doi.org/10.1016/j.biomaterials.2014.02.020.

References

[1] Cowin SC, Doty SB. Tissue mechanics. Springer; 2007.
[2] Fung YC. Biomechanics: mechanical properties of living tissues. 2nd ed. Springer; 1993.
[3] Atala A, Kasper FK, Mikos AG. Engineering complex tissues. Sci Transl Med 2012;4:160rv12.
[4] Freed LE, Guilak F, Guo XE, Gray ML, Tranquillo R, Holmes JW, et al. Advanced tools for tissue engineering: scaffolds, bioreactors, and signaling. Tissue Eng 2006;12:3285–305.

[5] Butler DL, Goldstein SA, Guilak F. Functional tissue engineering: the role of biomechanics. J Biomech Eng 2000;122:570–5.
[6] Neidert MR, Tranquillo RT. Tissue-engineered valves with commissural alignment. Tissue Eng 2006;12:891–903.
[7] Schutte SC, Chen Z, Brockbank KG, Nerem RM. Cyclic strain improves strength and function of a collagen-based tissue-engineered vascular media. Tissue Eng Part A 2010;16:3149–57.
[8] Lee KW, Stolz DB, Wang Y. Substantial expression of mature elastin in arterial constructs. Proc Natl Acad Sci U S A 2011;108:2705–10.
[9] Auger FA, D'Orléans-Juste P, Germain L. Adventitia contribution to vascular contraction: hints provided by tissue-engineered substitutes. Cardiovasc Res 2007;75:669–78.
[10] Huang D, Chang TR, Aggarwal A, Lee RC, Ehrlich HP. Mechanisms and dynamics of mechanical strengthening in ligament-equivalent fibroblast-populated collagen matrices. Ann Biomed Eng 1993;21:289–305.
[11] Sander EA, Stylianopoulos T, Tranquillo RT, Barocas VH. Image-based multiscale modeling predicts tissue-level and network-level fiber reorganization in stretched cell-compacted collagen gels. Proc Natl Acad Sci U S A 2009;106:17675–80.
[12] Costa KD, Lee EJ, Holmes JW. Creating alignment and anisotropy in engineered heart tissue: role of boundary conditions in a model three-dimensional culture system. Tissue Eng 2003;9:567–77.
[13] Aubin H, Nichol JW, Hutson CB, Bae H, Sieminski AL, Cropek DM, et al. Directed 3D cell alignment and elongation in microengineered hydrogels. Biomaterials 2010;31:6941–51.
[14] Grinnell F, Petroll WM. Cell motility and mechanics in three-dimensional collagen matrices. Annu Rev Biomed Eng 2010;26:335–61.
[15] Shi Y, Vesely I. Fabrication of mitral valve chordae by directed collagen gel shrinkage. Tissue Eng 2003;9:1233–42.
[16] Nirmalanandhan VS, Levy MS, Huth AJ, Butler DL. Effects of cell seeding density and collagen concentration on contraction kinetics of mesenchymal stem cell-seeded collagen constructs. Tissue Eng 2006;12:1865–72.
[17] Liu JY, Swartz DD, Peng HF, Gugino SF, Russell JA, Andreadis ST. Functional tissue-engineered blood vessels from bone marrow progenitor cells. Cardiovasc Res 2007;75:618–28.
[18] Nerem RM, Seliktar D. Vascular tissue engineering. Annu Rev Biomed Eng 2001;3:225–43.
[19] Xu T, Zhao W, Zhu JM, Albanna MZ, Yoo JJ, Atala A. Complex heterogeneous tissue constructs containing multiple cell types prepared by inkjet printing technology. Biomaterials 2013;34:130–9.
[20] Roth EA, Xu T, Das M, Gregory C, Hickman JJ, Boland T. Inkjet printing for high-throughput cell patterning. Biomaterials 2007;25:3707–15.
[21] Gurkan UA, Fan Y, Xu F, Erkmen B, Urkac ES, Parlakgul G, et al. Simple precision creation of digitally specified, spatially heterogeneous, engineered tissue architectures. Adv Mater 2013;25:1192–8.
[22] Zhao R, Boudou T, Wang WG, Chen CS, Reich DH. Decoupling cell and matrix mechanics in engineered microtissues using magnetically actuated microcantilevers. Adv Mater 2013;25:1699–705.
[23] Legant WR, Chen CS, Vogel V. Force-induced fibronectin assembly and matrix remodeling in a 3D microtissue model of tissue morphogenesis. Integr Biol 2012;4:1164–74.
[24] Sakar MS, Neal D, Boudou T, Borochin MA, Li Y, Weiss R, et al. Formation and optogenetic control of engineered 3D skeletal muscle bioactuators. Lab Chip 2012;12:4976–85.
[25] Hinz B, Gabbiani G. Fibrosis: recent advances in myofibroblast biology and new therapeutic perspectives. F1000 Biol Reports 2010;2:78.
[26] Boudou T, Legant WR, Mu A, Borochin MA, Thavandiran N, Radisic M, Zandstra PW, et al. A microfabricated platform to measure and manipulate the mechanics of engineered cardiac microtissues. Tissue Eng Part A 2012;18:910–9.
[27] Tomasek JJ, Gabbiani G, Hinz B, Chaponnier C, Brown RA. Myofibroblasts and mechano-regulation of connective tissue remodelling. Nat Rev Mol Cell Biol 2002;3:349–63.
[28] Gabbiani G. The myofibroblast in wound healing and fibrocontractive diseases. J Pathol 2003;200:500–3.
[29] Legant WR, Pathak A, Yang MT, Deshpande VS, McMeeking RM, Chen CS. Microfabricated tissue gauges to measure and manipulate forces from 3D microtissues. Proc Natl Acad Sci U S A 2009;106:10097–102.
[30] Zhao R, Simmons CA. An improved texture correlation algorithm to measure substrate-cytoskeletal network strain transfer under large compressive strain. J Biomech 2012;45:76–82.
[31] Hinz B. Formation and function of the myofibroblast during tissue repair. J Invest Dermatol 2007;127:526–37.
[32] Levental KR, Yu H, Kass L, Lakins JN, Egeblad M, Erler JT, et al. Matrix crosslinking forces tumor progression by enhancing integrin signaling. Cell 2009;139:891–906.
[33] Georges PC, Hui JJ, Gombos Z, McCormick ME, Wang AY, Uemura M, et al. Increased stiffness of the rat liver precedes matrix deposition: implications for fibrosis. Am J Physiol Gastrointest Liver Physiol 2007;293:G1147–54.
[34] Woodley DT, Yamauchi M, Wynn KC, Mechanic G, Briggaman RA. Collagen telopeptides (cross-linking sites) play a role in collagen gel lattice contraction. J Invest Dermatol 1991;97:580–5.
[35] Goffin JM, Pittet P, Csucs G, Lussi JW, Meister JJ, Hinz B. Focal adhesion size controls tension-dependent recruitment of alpha-smooth muscle actin to stress fibers. J Cell Biol 2006;172:259–68.
[36] Mammoto T, Ingber DE. Mechanical control of tissue and organ development. Development 2010;137:1407–20.
[37] Juncosa-Melvin N, Boivin GP, Galloway MT, Gooch C, West JR, Butler DL. Effects of cell-to-collagen ratio in stem cell-seeded constructs for Achilles tendon repair. Tissue Eng 2006;12:681–9.
[38] Wakatsuki T, Kolodney MS, Zahalak GI, Elson EL. Cell mechanics studied by a reconstituted model tissue. Biophys J 2000;79:2353–68.